J. Biomed. Eng. Res : 110-116, 2006

MRI Content-Adaptive Finite Element Mesh Generation Toolbox

W. H. Lee, T.-S. Kim, M. H. Cho, S. Y. Lee

Functional and Metabolic Imaging Center
Department of Biomedical Engineering, Kyung Hee University,
Yongin, Kyungki, Republic of Korea
(Received May 4, 2006. Accepted June 2, 2006)

Abstract

Finite element method (FEM) provides several advantages over other numerical methods such as boundary element method, since it allows truly volumetric analysis and incorporation of realistic electrical conductivity values. Finite element mesh generation is the first requirement in such in FEM to represent the volumetric domain of interest with numerous finite elements accurately. However, conventional mesh generators and approaches offered by commercial packages do not generate meshes that are content-adaptive to the contents of given images. In this paper, we present software that has been implemented to generate content-adaptive finite element meshes (cMESHes) based on the contents of MR images. The software offers various computational tools for cMESH generation from multi-slice MR images. The software named as the Content-adaptive FE Mesh Generation Toolbox runs under the commercially available technical computation software called Matlab. The major routines in the toolbox include anisotropic filtering of MR images, feature map generation, content-adaptive node generation, Delaunay tessellation, and MRI segmentation for the head conductivity modeling. The presented tools should be useful to researchers who wish to generate efficient mesh models from a set of MR images. The toolbox is available upon request made to the Functional and Metabolic Imaging Center or Bio-imaging Laboratory at Kyung Hee University in Korea.

Key words : finite element method, MRI, content-adaptive mesh generation toolbox

I. INTRODUCTION

Finite element method (FEM) is an efficient and powerful means to solve electromagnetic problems as well as compute the solutions of complex differential equations. FEM is widely used in various fields such as biomechanical analysis of surgery or bioelectromagnetic source imaging [1, 2].

FEM is getting more popular in many biomedical applications due to (1) readily available CT or MR images where geometrical shape information can be derived, (2) recent developments in measuring electrical or thermal conductivity information which can be incorporated in to the FE models, (3) numerical power that allows truly volumetric analysis, and (4) much improved computing power of modern computers.

To apply FEM to bioelectromagnetic problems, one of the major requirements is the mesh generation of an electrically conducting volume. There have been numerous attempts to develop effective and efficient mesh generation methods for volumes with complex geometry. For instance, Ziolkowski and Brauer reported a method for 2-D FE mesh generation, but they used an equidistant technique resulting in over-sampled elements [2]. Hartmann and Kruggel [3] also reported a fast technique for mesh generation using bigger bricks to represent homogeneous regions and sub-bricks for smaller regions. Most conventional mesh generation schemes utilized the uniform meshes where FE elements of relatively same size are used to represent a complex volume [4, 5]. One of the disadvantages of these approaches is overly created finite elements, resulting in the overwhelming computational load, although the procedure to generate FE meshes is simple and user-friendly. In addition, there exist several commercial packages offering a means of producing standardized FE mesh models including COMSOL [6] and Nastran [7], and research projects such as the Scientific Computing and Imaging [8] and QMG Project [9].

Although these techniques offer their own advantages in generating FE meshes, their capability for generating adequate mesh models of complex volumes presents the following

This study was supported by a grant of the Korea Health 21 R&D Project, Ministry of Health and Welfare, Republic of Korea (02-PJ3-PG6-EV07-0002).
Corresponding Author : Tae-Seong Kim, Ph.D.
Functional and Metabolic Imaging Center, Department of Biomedical Engineering, Kyung Hee University 1 Seocheon-dong, Giheung-gu, Yongin-si, Gyeonggi-do Republic of Korea, 446-701
Tel : +82-31-201-3731
E-mail : tskim@khu.ac.kr

limitations. First, most commercial mesh generators cannot handle arbitrary geometry of complex biological shapes requiring much simplification of complicated boundaries. Second, most mesh generation techniques do not utilize the content of image features when generating meshes, requiring more elements to represent fine structures with much smaller elements. This requires careful supervision of users and manual control to generate nodes especially for complex biological volumes. Third, most mesh generation schemes tend to produce over-sampled elements to represent small regions. This tends to result in the increased number of nodes and elements, thus increasing computational load of the FE method. Although more efficient computation techniques [10] for the FE analysis are being introduced, there is a strong demand for faster, more efficient and effective, and possibly automatic mesh generator to reduce the computational load of the FE method. Reducing the number of finite elements, while maintaining the numerical accuracy of the FE analysis, could be an outstanding benefit to FEM applications.

In that respect, one critical attribute of novel mesh generation scheme can be content-adaptiveness of meshes to the features of images or volumes of different geometries from individuals. Recently, we developed an efficient and improved content-adaptive mesh generation technique [11]. This technique was based on the original framework of [12]. In our work, we made the technique more efficient by incorporating two additional features. First, we utilized the content-enhancing anisotropic diffusion for pre-segmentation of sub-volumes and improvement in the quality of the feature maps. Second, we proposed more efficient and accurate content-adaptive node generations schemes.

In this paper, we introduce a software package that generates cMESHes according to our developed techniques. The software, named as the Content-adaptive FE Mesh Generation Toolbox, was implemented using a commercially available computational package called Matlab [13] with GUI interface. The package is available to those who wish to use it in their FE analysis under the GNU General Public License [14] upon request made to Functional and Metabolic Imaging Center [15] or Bio-imaging Lab [16].

The toolbox follows three main steps: the first includes morphological preprocessing of MR images for background segmentation; the second the edge-preserving enhancement of MR images via anisotropic filtering; the third the cMESH generation via feature map generation, digital halftoning, and Delaunay tessellation. Each part is accompanied with a visualization tool to allow examination of each outcome. Details of usage of the toolbox are summarized in the paper.

As a demonstration, we show several 2-D and 3-D cMESH models of the human head from a set of MR images. A potential application of this package is the forward and inverse computations of bioelectromagnetic problems of E/MEG source imaging [17].

II. METHODS AND RESULTS

Main Panel

By invoking the toolbox under Matlab, the main panel of the cMESH generator appears as shown in Fig. 1. Three major groups include MRI Preprocessing, Finite Element Head Modeling, and Head Conductivity Modeling.

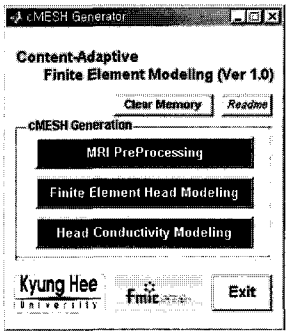

Fig. 1. Main panel of the content-adaptive FE mesh generation toolbox showing three main groups of tools.

A. MRI Preprocessing Group

To extract the head regions only, morphological processing tools for binary mask images of MRI are available. The MRI preprocessing panel appears as shown in Fig. 2 by invoking MRI PreProcessing.

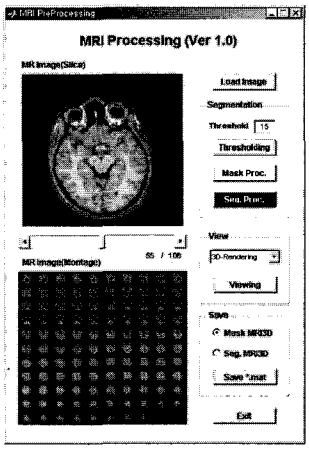

Fig. 2. The MRI processing tool in the content-adaptive FE mesh generator. Results of morphological processing are shown in the single-slice view and montage view windows. The upper shows the segmented single MR image and the bottom a set of multi-slice MR images simultaneously.

Loading of 3-D MRI Volumes: Load Image

A set of multi-slice anatomical MR images covering the whole head can be loaded into the toolbox by invoking Load Image.

MR Background Removal: Segmentation

To remove the background other than the head region, morphological processing including thresholding, opening, and closing of the head binary masks was performed. The value of threshold to create the binary mask MR image is controlled by users under Thresholding. With the obtained binary masks, morphological processing to remove the noise and artifacts of the background except the head regions is employed automatically under Mask Proc. and Seg. Proc. This multi-slice volume set of MR images is subsequently used in further processing of content-adaptive mesh generation.

Visualization: View

This function shows three optional choices to visualize the images in three different views: 3D-rendering for a surface-rendered view of the selected volume, montage for a simultaneous view of all slices, and contour-slices for 3-D views of each slice with a gap.

Saving of 3-D MRI Volumes: Save

This save option saves binary mask and segmented images of 3-D MRI. Users can choose the saving category of 3-D MRI volumes under Mask MRI3D and Seg. MRI3D. These different types of MR images are used later in cMESH generation and MRI segmentation for the head conductivity modeling.

B. Finite Element Head Modeling Group

To generate cMESHes from the preprocessed head regions, the finite element head modeling panel appears as shown in Fig. 3 by invoking Finite Element Head Modeling.

Loading of 3-D MRI Volumes: Load Image

A set of segmented MR volume images, preprocessed by the toolbox, as in Fig. 2 can be loaded into the toolbox by invoking Load Image.

Image Resize Setup: Image Selecting

With this option, the loaded set of images can be resized according to users' specification. This option is added in case of reducing the volume, thereby reducing the number of nodes and element. The image selecting parameters include the size and range of images: users can input the row and column numbers to resize the MR images accordingly. To select MR image slices, the following parameters can be adjusted by users: Start, Gap, and End that decide which MR slices are passed into the 2-D and 3-D processing of cMESH generation by invoking Resize. Users can examine the selected MR slices by moving up and down the slider. The selected MR images are subsequently used in the cMESH generation.

Computation: Get Nodes

-3-D Gradient Vector Flow Anisotropic Diffusion Filtering

In order to remove undesirable objects in the given MR images including noise and artifacts and to pre-segment anatomical regions, we applied the 3-D Gradient Vector Flow (GVF) anisotropic diffusion algorithm. The GVF nonlinear diffusion, which we successfully applied to regularize diffusion tensor MR images previously [18], is proven to be

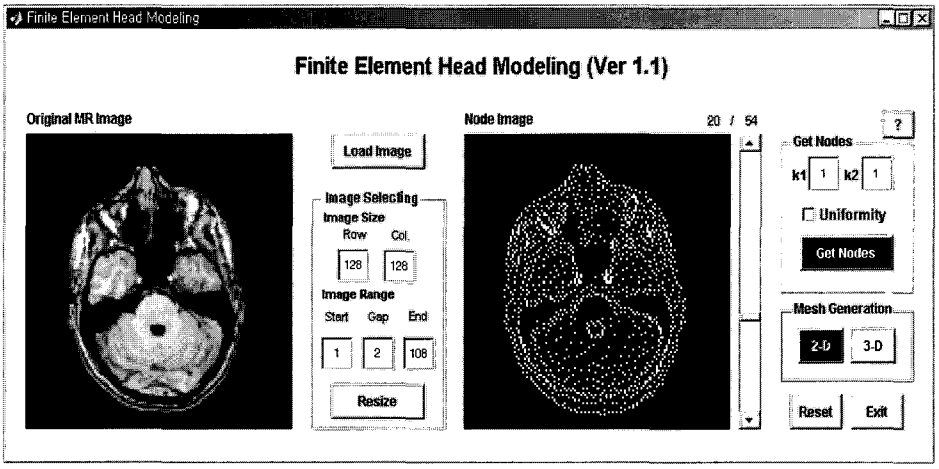

Fig. 3. Finite element head modeling tool in the content-adaptive FE mesh generator. Results of 2-D content-adaptive mesh nodes are shown. The left shows the original MR image and the right content-adaptive mesh nodes.

much more robust than conventional structure tensor-based anisotropic diffusion algorithm [19] and can be summarized as follows.

The GVF as a 3-D vector field can be defined as,

$$V(x,y,z) = (u(x,y,z), v(x,y,z), w(x,y,z)). \quad (1)$$

The field can be obtained by minimizing the energy functional:

$$\begin{aligned} \varepsilon &= \iiint \gamma(\eta_u + \eta_v + \eta_w) + |\nabla f|^2 |V - \nabla f|^2 \partial x \partial y \partial z \\ \eta_u &= u_x^2 + u_y^2 + u_z^2 \\ \eta_v &= v_x^2 + v_y^2 + v_z^2 \\ \eta_w &= w_x^2 + w_y^2 + w_z^2 \end{aligned} \quad (2)$$

where f is an image edge map and γ is a noise control parameter.

For 3D anisotropic smoothing, the structure tensor S is formed with the components of V,

$$S = V(V)^T \quad (3)$$

The 3D anisotropic regularization is governed using the GVF diffusion tensor DGVF which is constructed with eigen components of S:

$$\partial J / \partial t = div[D_{GVF} \nabla J] \quad (4)$$

where J is an image volume in 3-D. The regularization behavior of Eq. (4) is controlled with the eigenvalue analysis of the GVF structure tensor.

It should be noted that this step is essential to prevent the generation of unnecessary and spurious nodes. Any anisotropic diffusion scheme can be used other than what we used in this step. We also have added an option for the conventional anisotropic diffusion method [19] for faster execution of this functional. The diffusivity (i.e., smoothing) of anisotropic filtering can be adjusted by controlling the input parameter k1.

－Feature Map Generation

To derive content-adaptive mesh nodes from an image, a feature map is generated from an image utilizing the structure tensor matrix S as we proposed in [11]

The structure tensor is expressed as,

$$S = \begin{bmatrix} I_x^2 & I_x I_y \\ I_y I_x & I_y^2 \end{bmatrix} \quad (5)$$

where I is an image and x and y are row and column-wise spatial derivates.

The feature map is then derived from the eigen components of the above the structure tensor.

$$f_S(i,j) = \sqrt{(\mu_1^S(i,j) \pm \mu_2^S(i,j))} \quad (6)$$

where μ's are the positive eigenvalues of the structure tensor matrix and i and j are image indices . This map reflects the edges and corners of image structures for the plus sign and the local coherence or anisotropy for the minus sign [20]. Other measures such as mean curvature [21] could be used as a feature extractor in accordance with the need of applications.

Finally, the sensitivity of feature map is controlled by converting the feature map using the parameter, as shown below,

$$f'(i,j) = f(i,j)^{1/\kappa}. \quad (7)$$

where the parameter k has been implemented in the toolbox as k2.

－Content-Adaptive Node Sampling Via Digital Halftoning

In order to sample content-adaptive mesh nodes from the feature map, we used a popular halftoning algorithm as suggested in the original work of Lee et al. [11]. The Floyd-Steinberg error diffusion algorithm [22] was implemented with the serpentine scanning. This is an effective tool to be used to generate mesh nodes according to the information in the feature map. The goal is to distribute mesh nodes according to the density of feature maps such that node density is proportional to the content image features. The result is that the mesh nodes are automatically created according to the given MR image features with the desired property in that the node spatial density is proportional to the magnitude of the second directional directive of the image. In this way, the mesh nodes are produced in a manner of nonuniform sampling (i.e., the local density of sample adapts to the local frequency content of the MR images). There exists much advanced halftoning algorithms [23] which could be used instead, although they are not implemented in the toolbox.

Mesh Generation Via Delaunay Tessellation

—2-D Content-Adaptive Mesh Generation: 2D

Before cMESH generation, physical dimensions can be assigned to the sampled nodes by invoking Field of View. The parameters of this option take In-plain Distance, Slice Thickness, and Slice Gap as shown in Fig. 4 (a) to convert the distance of sampled nodes into proper physical units in mm and so as to slice thickness and slice gaps.

Once the content-adaptive nodes were generated from the procedures mentioned above, mesh generation of triangular elements in 2-D is achieved using the Delaunay tessellation algorithm [24]. The Delaunay triangulation connects given mesh nodes in a way that the circle circumscribing any triangular element contains only the nodal points belonging to that triangle [13]. The Delaunay triangulation yields a well-structured cMESHes at a reasonable computational cost.

As mentioned previously, the cMESH generation scheme should place small elements in high frequency regions of an image, while larger elements should be used in low frequency regions. This creates fine FE elements in the complex regions and coarse elements in the uniform or feature-free regions.

Fig. 4 (a) shows the feature map derived from Eq. (6) with the plus sign and their corresponding cMESHes in Fig. 4 (b). There are 1614 nodes and 3139 elements. The result clearly demonstrates that the implemented toolbox produces adaptive FE meshes to the contents of the given MRI. That is bigger elements are present in the homogeneous regions and smaller elements in the high frequency regions.

Fig. 5 (a) displays the information panel with the three parameters to control the physical dimension of the sampled nodes. Fig. 5 (b) shows a viewing panel of 2-D cMESHes with options to save mesh data. The mesh save option saves the

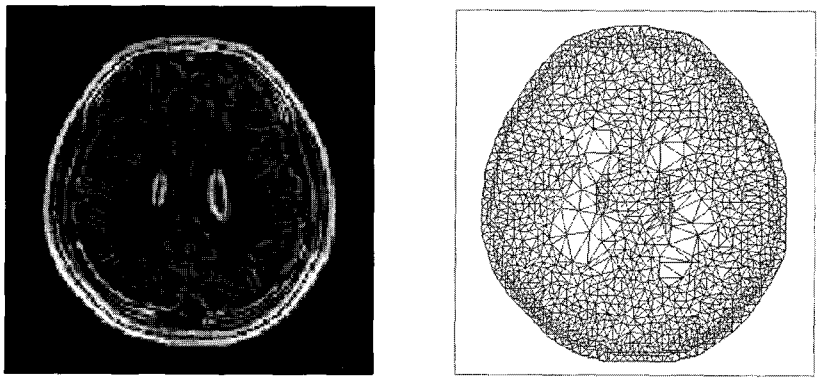

(a) (b)

Fig. 4. (a) Feature map using Eq. (6) and (b) cMESHes from (a) with 1614 nodes and 3139 elements

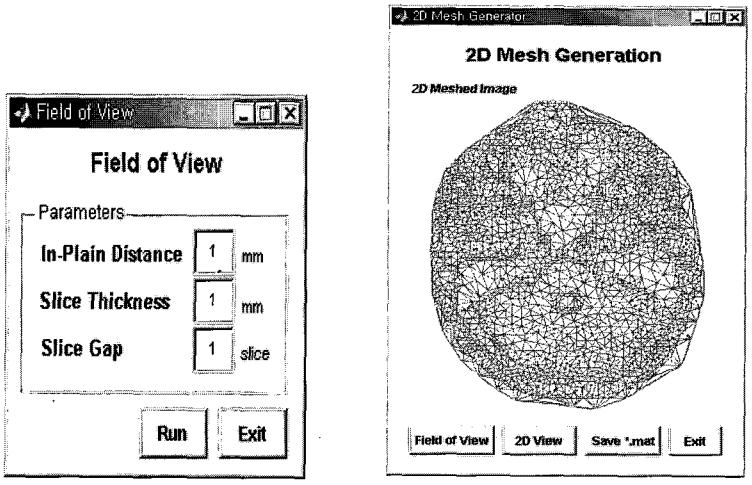

(a) (b)

Fig. 5. (a) Input field panel of MR imaging parameters for in-plane node distance, slice thickness, and slice gap and (b) cMESH display panel of 2-D content-adaptive mesh generator.

node locations and node connectivity matrix such that they can be used in any FE solvers.

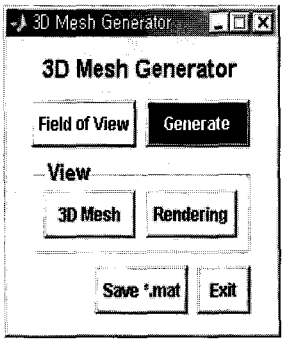

Fig. 6. 3-D content-adaptive mesh generator by involving the 3-D Mesh Generator.

—3-D Content-Adaptive Mesh Generation: 3D

Fig. 6 shows the 3-D content-adaptive mesh generator by invoking 3D. Once the content-adaptive nodes were generated in 3-D slice by slice, mesh generation of tetrahedral elements in 3-D gets done using the same Delaunay tessellation procedure in a straightforward extension of the 2-D technique.

Fig. 7 (a) is the surface rendered MR volume to be meshed. Fig. 7 (b) shows the 3-D cMESHes generated using the implemented toolbox. There are 8342 nodes and 46830 tetrahedral elements. The characteristics of content-adaptive meshes are clearly presented on the top slice of the head.

Resetting the Toolbox: Reset

The processed data can be reset by users to change cMESH results by invoking Reset.

C. Head Conductivity Modeling Group

The toolbox also includes tools for electrical conductivity modeling.

To model the head with sub-regions with isotropic conductivity, MR images must be segmented into anatomically distinct regions: five sub-regions including white matter (WM), gray

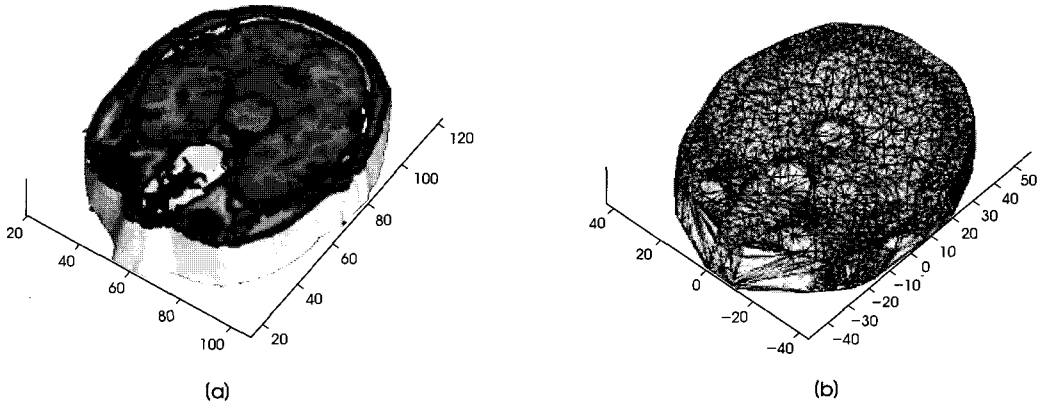

Fig. 7. (a) 3-D surface rendered head volume of MRI to be meshed and (b) 3-D content-adaptive meshes with 8342 nodes and 46830 tetrahedral elements generated using the implemented toolbox.

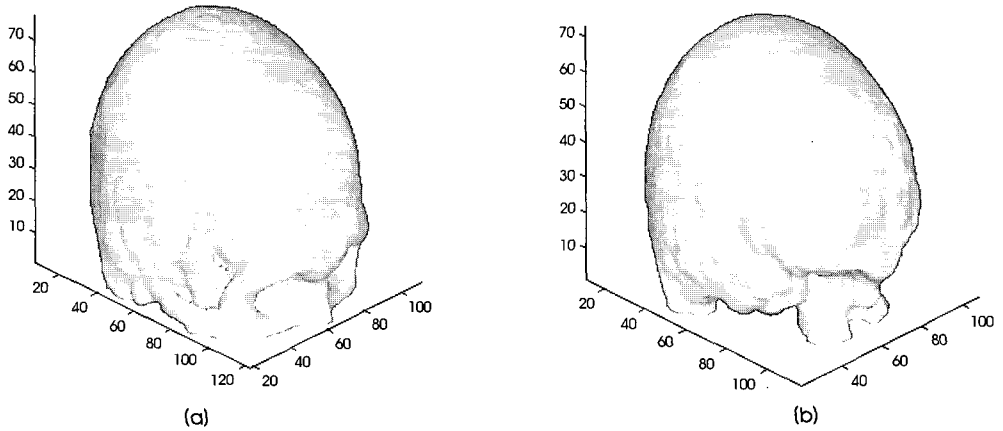

Fig. 8. (a) 3-D surface rendered outer skull and (b) inner skull.

matter (GM), CSF, skull, and scalp are common in E/MEG forward and inverse problems. To assist such modeling, the toolbox is designed to take the output files from BrainSuite [25] which is available free of charge and does excellent job of extracting WM, GM, and CSF; but it does not produce masks for skull and scalp. Recently, a technique has been developed to extract skull from MR images [26]. We have implemented this method and incorporated into the toolbox. Fig. 8 (a) and (b) shows the outer and inner skull surface from our implemented tool. Our modeling tool produces conductivity maps for each MR slice. Proper isotropic conductivity values can be assigned to each sub-region by users.

III. DISCUSSION AND CONCLUSION

We have presented the MRI Content-adaptive Finite Element Mesh Generation Toolbox and its major routines. The toolbox contains various sub-routines that are used to generate FE meshes that are content-adaptive to given MR images or volumes.

The toolbox described in the paper is the first release of a software tool that can be used in various fields where FEM is applicable. We hope it becomes a useful simulation or practical tool to the FEM community and to those who conduct research via FE analysis. In our research, we are currently investigating the effect of cMESHes on the accuracy of FE analysis via bioelectromagnetic forward solutions and the preliminary results are presented in [27].

Next versions of the toolbox, when it becomes available, will be announced and made available on our web site [15, 16]. We would appreciate any feedback form users.

REFERENCES

[1] E. Molinari, M.Fato, G. De Leo, D. Riccardo, and F. Beltrame, "Simulation of the biomechanical behavior of the skin in virtual surgical applications by finite element methods," *IEEE Trans. Biomed. Engi.*, 2005.

[2] M. Ziolkowski, and H. Brauer, "Methods of mesh generation for biomagnetic problems," *IEEE Trans. Magnetics,* vol. 32, no. 3, pp. 1345-1348, 1996.

[3] U. Hartmann, and F. Kruggel, "A fast algorithm for generating large tetrahedral 3D finite element meshes from magnetic resonance tomograms," in *Proc. IEEE Biomed. Image Analysis,* St. Barbara, 1998, pp. 184-192.

[4] T.-S.Kim, Y. Zhou, S. Kim, and M. Singh, "EEG distributed source imaging with a realistic finite element head model," *IEEE Trans. Nucl. Sci.*, vol. 49, no. 3, pp. 745-752, 2002.

[5] S. Kim, T.-S. Kim, Y. Zhou, and M. Singh, "Influence of conductivity tensors on the scalp electrical potential: study with 2-D finite element models," *IEEE Trans. Nucl. Sci.*, vol. 50, no. 1, pp. 133-138, 2003.

[6] http://www.comsol.com/

[7] http://www.nenastran.com/

[8] http://www.sciutah.edu/

[9] http://www.cs.cornell.edu/Info/People/vavasis/qmghome.html/

[10] C. H. Wolters, M. Kuhn, A. Anwander, and S. Reitzinger, "Fast anisotropic high resolution finite element head modeling in EEG/MEG source localization," in *Proc. Int. Conf. Biomag.*, Aug. 2002.

[11] W. H. Lee, T.-S. Kim, M. H. Cho, and S. Y. Lee, "Content-adaptive finite element mesh generation of 3-D complex MR volumes for bioelectromagnetic problems," in *Proc. 27th Ann. Int. Conf. IEEE EMBS*, Shanghai, China, Sept. 2005.

[12] Y. Yang, M. N. Wernick, and J. G. Brankov, "A fast approach for accurate content-adaptive mesh generation," *IEEE Trans. Image Processing*, vol. 12, no. 8, pp. 866-881, 2003.

[13] http://www.mathworks.com/

[14] http://www.gnu.org/

[15] http://web.kyunghee.ac.kr/~fmic/

[16] http://bioimage.khu.ac.kr/

[17] N. Gener and C. E. Acar, "Sensitivity of EEG and MEG measurements to tissue conductivity," *Phys. Med. Biol.*, vol. 49, pp. 701-717, 2004.

[18] T.-S. Kim, S. Kim, D. Huang, and M. Singh, "DT-MRI Regularization using 3D nonlinear gradient vector flow anisotropic diffusion," in *Proc. Int. Conf. IEEE Eng. Med. Biol.*, 2004, pp. 1880-1883.

[19] J. Weickert, "A review of nonlinear diffusion filtering," *Scale-Space Theory in Computer Vision, Lecture Notes in Computer Science*, vol. 1252, Springer, Berlin, pp. 3-28, 1997.

[20] D. Tschumperle and R. Deriche, "Diffusion PDEs on vector-valued images," *IEEE Sig. Proc. Mag.*, Sep., pp. 16-25, 2002.

[21] K. Z. Abd-Elmoniem, A.-B. Youssef, and Y. M. Kadah, "Real-time speckle reduction and coherence enhancement in ultrasound imaging via nonlinear anisotropic diffusion," *IEEE Trans. Biomed. Engi.*, vol. 49, no. 9, pp. 997-1014, 2002.

[22] R. Floyd and L. Steinberg, "An adaptive algorithm for spatial gray scale," in *Proc.* Int. Symp. Digest of Tech. Papers, pp. 36-37, 1975.

[23] I. Katsavounidis and C.-C. J. Kuo, "A multiscale error diffusion technique for digital halftoning," *IEEE Trans. Image Processing,* vol. 6, no. 3, 483-490, 1997.

[24] D. F. Watson, "Computing the n-dimensional Delaunay tessellation with application to Voronoi polytypes", *The Comp. Jour.*, vol. 24, no. 2, pp. 167-172, 1981.

[25] http://brainsuite.usc.edu/

[26] B. Dogdas, D. W. Shattuck, and R. M. Leahy, "Segmentation of skull and scalp in 3-D human MRI using mathematical morphology," *Human Brain Mapping*, vol.26, pp.273-285, 2005.

[27] W. H. Lee, J. S. Moon, S. Y. Lee, and T.-S. Kim, "Numerical evaluation of MRI content-adaptive finite element models via EEG forward solutions," in *Proc. World Congress on Medical Physics and Biomedical Engineering*, Seoul, Korea, 2006.